TISSUE ENGINEERING: Part C
Volume 22, Number 3, 2016

DOI: 10.1089/ten.tec.2015.0334

termis
Tissue Engineering
& Regenerative Medicine
International Society

METHODS ARTICLE

Fluid Flow Regulation of Revascularization and Cellular Organization in a Bioengineered Liver Platform

Pedro M. Baptista, PharmD, PhD,[1–4,*] Emma C. Moran, PhD,[1,*] Dipen Vyas, PhD,[1] Maria H. Ribeiro, PhD,[5] Anthony Atala, MD,[1] Jessica L. Sparks, PhD,[6] and Shay Soker, PhD[1]

Objective: Modeling of human liver development, especially cellular organization and the mechanisms underlying it, is fundamental for studying liver organogenesis and congenital diseases, yet there are no reliable models that mimic these processes *ex vivo*.
Design: Using an organ engineering approach and relevant cell lines, we designed a perfusion system that delivers discrete mechanical forces inside an acellular liver extracellular matrix scaffold to study the effects of mechanical stimulation in hepatic tissue organization.
Results: We observed a fluid flow rate-dependent response in cell distribution within the liver scaffold. Next, we determined the role of nitric oxide (NO) as a mediator of fluid flow effects on endothelial cells. We observed impairment of both neovascularization and liver tissue organization in the presence of selective inhibition of endothelial NO synthase. Similar results were observed in bioengineered livers grown under static conditions.
Conclusion: Overall, we were able to unveil the potential central role of discrete mechanical stimulation through the NO pathway in the revascularization and cellular organization of a bioengineered liver. Last, we propose that this organ bioengineering platform can contribute significantly to the identification of physiological mechanisms of liver organogenesis and regeneration and improve our ability to bioengineer livers for transplantation.

Introduction

Liver organogenesis and regeneration are both highly complex processes that involve the coordination of numerous cells types and signals resulting in cellular organization. Better modeling of this process is key in understanding liver development and regeneration. Due to the limitations of animal models, including cost and ethical considerations, the current approach to study these complex phenomena is by modeling these processes in *ex vivo* systems. Since development of the vascular system is essential for liver development and regeneration, these *ex vivo* models should also include a vascular component.[1–6]

In vitro models have been developed in the past decades to mimic organ development and regeneration, but most employ cells cultured in two-dimensional (2D) plastic dishes and do not recapitulate the native three-dimensional (3D) organ structure. The available 3D tissue culture models are mostly static and do not incorporate the mechanical effects of fluid flow. On the other hand, microfluidic systems are used for external perfusion of small tissue constructs and thus lack true physiological organ perfusion properties.[7]

The emergence of novel decellularization/recellularization techniques has recently been employed by us and others to create whole organ scaffolds, including livers, for organ bioengineering.[8–13] Owing to the preservation of the vascular tree architecture within these acellular organ scaffolds, they support whole organ perfusion, which can be used for cell seeding and maintenance. In addition, the vascular perfusion network can be used to simulate the effect of fluid flow-derived mechanical forces on specific cell populations. Finally, the acellular scaffolds contain the native tissue microenvironment, including the composition and arrangement of the liver extracellular matrix (ECM). Despite recent advances in whole liver engineering, optimized conditions for cell seeding, tissue growth and organization, as well as the mechanisms governing these processes, are largely unknown.

[1]Wake Forest Institute for Regenerative Medicine, Wake Forest University Health Sciences, Winston-Salem, North Carolina.
[2]University of Zaragoza, Zaragoza, Spain.
[3]IIS Aragón, CIBERehd, Zaragoza, Spain.
[4]Aragon Health Sciences Institute (IACS), Zaragoza, Spain.
[5]Faculty of Pharmacy, Research Institute for Medicines (iMed.ULisboa), University of Lisbon, Lisbon, Portugal.
[6]Department of Chemical, Paper and Biomedical Engineering, Miami University, Oxford, Ohio.
*These authors contributed equally to this work.

In the current study, we used an *in vitro* bioengineered intact right liver lobe model[8,11] to study the effects of fluid flow mechanical stimulation on hepatic tissue organization. The precise control of flow rate/pressure in a perfusion bioreactor allowed us to determine the role of fluid flow in regulating cellular distribution and organization. To validate this platform, we used two cell lines that represent cell types within the liver, HepG2 hepatocytic cells and MS1 endothelial cells (EC), and confirmed the nitric oxide (NO) signaling pathway as a major mediator of shear stress-induced cellular organization. Collectively, our data suggest that a bioengineered liver, inside a customized perfusion bioreactor, can be used as a unique model to study the complexities of tissue organization *ex vivo*.

Materials and Methods

Liver ECM scaffold preparation

Briefly, ferret livers were decellularized as described by Baptista *et al.*[8] After decellularization, liver ECM scaffolds were prepared for each experiment by ligating and subsequently removing the left, caudate, and quadratic lobes, all ligated with 4-0 silk black-braided suture (Ethicon, Summerville, NJ). Scaffold reduction was performed to minimize the number of cells needed in experiments, as proof of concept. The remaining right lobe, cannulated through the portal vein with all the vascular structures intact, weighed between 3 and 4 g in all experiments. The scaffold was sterilized before use with a dose of 1.5 Mrad of gamma radiation by a cobalt-60 gamma irradiator (J. L. Shepherd and Associates, San Fernando, CA).

Bioreactor assembly

Bioreactor parts were sterilized with steam at 121°C and assembled in a sterile hood according to the diagram in Figure 1. Details of bioreactor parts and assembly can be found in the Supplementary Methods (Supplementary Data are available online at www.liebertpub.com/tec). Once connected, the bioreactor was placed in an incubator with 5% CO_2 at 37°C. Medium perfusion was started at 3 mL/min and preconditioning was performed overnight. System pressure was measured and recorded as described in the Supplementary Methods.

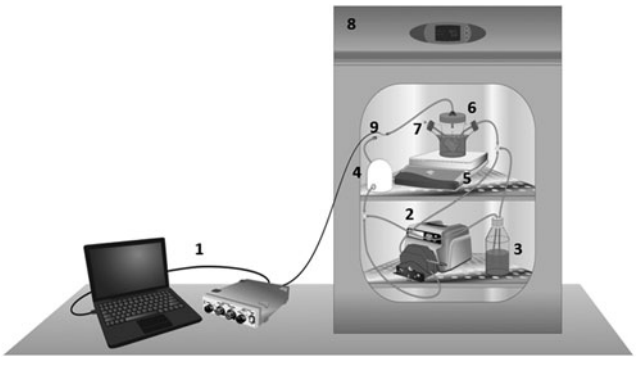

FIG. 1. A perfusion bioreactor system. Schematic diagram of a perfusion bioreactor system design; (1) pressure data measurement and recording, (2) peristaltic pump, (3) media reservoir, (4) pulse dampener, (5) magnetic stir-plate, (6) whole organ bioreactor in media, (7) cell injection port, (8) cell culture incubator, and (9) system pressure probe. A total of 6×10^7 cells are injected into the culture media and perfused into the portal vein inlet of the acellular liver ECM scaffold. ECM, extracellular matrix.

Cell seeding

To model hepatocytes, we used HepG2 cells, a well-differentiated human hepatocellular carcinoma line that retains many hepatocyte functions, including albumin secretion, and MS1 cells, a mouse endothelial line that exhibits many endothelial functions including expression of endothelial nitric oxide synthase (eNOS) and NO production, to model EC. A total of 60 million cells (30×10^6 HepG2 and 30×10^6 MS1 mouse EC) were seeded per scaffold at different flow rates (Supplementary Table S1). Cell seeding was carried through multiple intervals of cell injections into the culture media, with 4 h in between injections (Supplementary Table S1). These intervals were experimentally chosen based on the presence of a minute number of nonseeded cells in the media, under all seeding conditions. System perfusion at 6 mL/min delivers the cells into the scaffold through portal vein circulation.

The flow rates ranging from 3 to 12 mL/min were selected based on the physiological hepatic blood flow of an adult rat during rest (85 mL/min/Kg).[14,15] On an average, the 5–6-week old ferret livers, used to generate liver scaffolds, have a similar size and weight of an adult rat liver ($\sim$10 g for a 300 g Sprague–Dawley rat), and only the right lobe is used in these experiments, which is roughly one-third the weight of the whole liver. Taking this into consideration, the estimated physiologic portal flow rate for the liver scaffolds was 6 mL/min, which corresponds experimentally to a parenchymal fluid pressure of $\sim$3 mmHg, the physiologic value in most species.[16] The 40 mL/min flow rate was chosen as a high shear stress control.[17]

To maintain cell delivery constant and equivalent between conditions, the volume of culture medium and the total number of cells in the bioreactor vessel were adjusted (Supplementary Table S1) to allow a maximum cell delivery rate into the scaffold of $\sim$400,000 cells/min (this maximum cell delivery rate was found to be the best to avoid clogging through the scaffold's vascular network when compared with a higher cell delivery rate of 800,000 cells/min) (data not shown). The 40 mL/min flow rate was the exception to this condition due to medium volume constraints. Details of the cell seeding process can be found in the Supplementary Methods.

NO/prostaglandin inhibition and no flow experiments

All scaffolds were seeded at 9 mL/min using the same protocol described above, with $n=3$ for each condition. Twenty-four hours after seeding, media were changed in all bioreactors and one of three conditions was implemented. In the first condition, termed ''no flow bioreactor,'' perfusion of EGM-2 media was stopped and the scaffold remained in the bioreactor for 7 days in static conditions. In the L-NAME/Indomethacin experiments, the second condition, 1 mM of L-NAME and 50 μM of Indomethacin were added to the normal media to inhibit synthesis of NO and prostacyclin. This drug-supplemented media were changed every 24 h, to ensure constant activity of the drugs. The final

condition consisted of 9 mL/min control experiments, maintained with the standard conditions as described above. Glucose and pH were monitored throughout the 7-day period and media were collected on days 3 and 7. Details of the static culture control experiments can be found in the Supplementary Methods. All samples were collected after 7 days in the bioreactor for gene expression and histological analysis of tissue formation and organization.

Immunohistochemistry

Following fixation and tissue processing (details in Supplementary Methods), 5 μm histological sections were cut using a Leica microtome (Leica Biosystems, Buffalo Grove, IL) and hematoxylin and eosin stain was performed on sections of all bioreactors using an Autostainer XL (Leica Biosystems). Nuclear staining was performed with a solution of propidium iodide at 5 μg/mL in phosphate-buffered saline on sections of all experiments. Cell proliferation quantification was performed for all bioreactors by using immunofluorescence staining for *Ki-67* (Cat#. ab15580; Abcam, Cambridge, MA), followed by goat anti-rabbit Texas Red secondary antibody (Vector Labs, Burlingame, CA). Cellular apoptosis detection was performed using the TdT In Situ Apoptosis Detection Kit–Alexa Fluor 594 (R&D Systems, Minneapolis, MN) in all bioreactors. To identify each cell population in the bioscaffold, double immunofluorescence staining was performed for *eNOS* using mouse anti-eNOS (Cat#. 610297; BD Biosciences, San Jose, CA) and albumin (*ALB*) with goat anti-human albumin (Cat#. A80-229A; Bethyl Labs, Montgomery, TX) followed by donkey anti-mouse alexa fluor 594 and donkey anti-goat alexa fluor 488 (Invitrogen, Grand Island, NY). All sections were mounted in ProLong Gold Antifade Reagent with DAPI (Invitrogen). Details of image analysis methodology can be found in the Supplementary Methods.

Conditioned media assays

Media samples from 1-day experiments across all flow rates were taken and assayed for lactase dehydrogenase (LDH, Pierce LDH Cytotoxicity Assay Kit; Thermo Scientific, Waltham, MA). Cytotoxicity was then calculated by subtracting the LDH activity of the spontaneous LDH release control from the chemical-treated sample LDH activity, dividing by the total LDH activity, and multiplying by 100. Media samples collected from the control, NO/prostaglandin (PG) inhibition, and no flow conditions along with tissue culture controls on day 3 and 7 were analyzed using an NO (total) detection kit (EnzoLife Sciences, Farmingdale, NY) and Prostacyclin ELISA kit (Abnova, Walnut, CA).

RNA extraction and real-time polymerase chain reaction

Total RNA was extracted from a small sample of reseeded liver scaffolds using the Allprep DNA/RNA Mini Kit (Qiagen, Germantown, MD) with DNAse treatment. cDNA was synthesized from 500 ng of total RNA using Superscript III First Strand Synthesis (Life Technologies, Carlsbad, CA). Reverse transcription polymerase chain reaction (RT-PCR) was performed using Taqman Master Mix (Life Technologies) with mouse *KLF2*, *integrin β1*, *integrin β3*, and *eNOS* taqman probes with *GAPDH* housekeeping gene (Life Technologies). Expression of genes within a sample was normalized to *GAPDH* expression using the $2^{-\Delta Ct}$ method.

Statistics

Results are shown as mean ± standard deviation and statistical analysis was performed using Graphpad Prism v5 (Graphpad Software, Inc, La Jolla, CA). A series of one-way ANOVA's with *post-hoc* Bonferoni analysis were performed to determine differences between groups (i.e., across flow rates). Pearson's correlation coefficient was used to calculate statistically significant correlations between pressure measurements and quantitative outcomes.

Results

Influence of fluid flow-derived mechanical forces on cell seeding, proliferation, and viability

To study the mechanical effects of fluid flow on liver tissue organization, we used our previously published technique of whole liver bioengineering, using acellular ferret livers seeded with hepatocytic cell and EC.[8,18] This model provides two important features: (1) cells are situated inside a 3D ECM scaffolding system that mimics the native liver microarchitecture, biochemical and biomechanical environment and (2) it allows delivery of distinct fluid flow rates through the native liver vascular network. To control fluid flow parameters, the acellular liver scaffold is placed in a perfusion bioreactor equipped with a controllable pump and system pressure measurements with recording capabilities (Fig. 1 and Supplementary Methods).

To demonstrate cellular response to fluid flow-induced shear stress and pressures, we employed two commonly used hepatic and EC lines, HepG2 and MS1, respectively. Importantly, HepG2 cells express albumin and the metabolic enzymes of the cytochrome P450 family and are used extensively as a robust model in hepatocyte research; MS1 cells have typical EC phenotype and function and have helped in the past to characterize the regulation of the eNOS system.[19–22] For most studies described below, the acellular scaffolds were seeded with 60 million cells by perfusion at varying flow rates ranging from 3 to 12 mL/min, as described in Supplementary Table S1. These flow rates were chosen based on a ''physiological'' flow rate of ~6 mL/min for a liver with the volume and weight of the liver scaffold.[14]

To simulate the effects of high shear stress conditions, representing situations such as partial hepatectomy where hepatic blood flow to the remaining liver can reach nearly 10 times normal levels, additional scaffolds were seeded at 40 mL/min. Twelve hours postseeding, medium in the bioreactor was changed and continuous media perfusion was performed for an additional 1 or 7 days at the same flow rate used for cell seeding. Bioengineered liver constructs were harvested and analyzed at these time points.

Initial studies were focused on characterization of the physical aspects of the perfusion seeding system. Details of image analysis procedures can be found in Supplementary Methods. It was first demonstrated that there is a linear correlation between system pressure and flow rate for values of 3–12 mL/min (Fig. 2A). Cell penetration, determined by image analysis quantifying the distance between cell

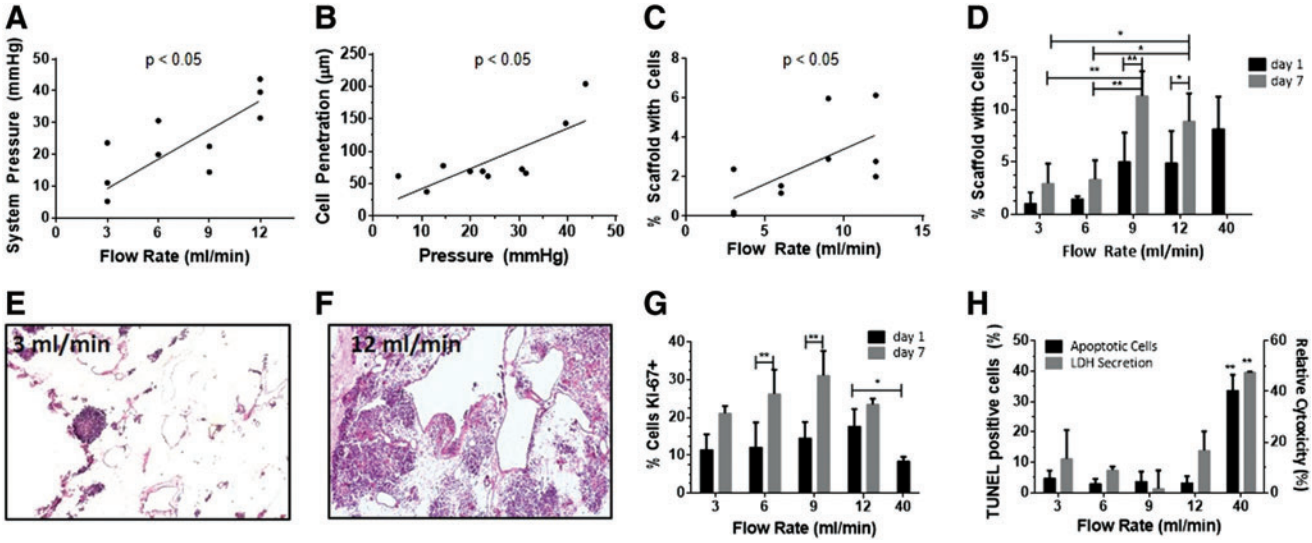

FIG. 2. Effect of flow rate and system pressures on cell deposition inside the liver ECM scaffold. **(A)** System (portal) pressure as a function of flow rate. **(B)** Image-based quantification of cell penetration into the scaffold as a function of system pressure. **(C)** Cell occupancy inside the scaffold as a function of flow rate, 1 day after cell seeding. **(D)** Cell occupancy as a function of flow rate after 1 or 7 days in the perfusion bioreactor. **(E, F)** Representative hematoxylin and eosin images of liver scaffolds after 1 day in the perfusion bioreactor postseeding at 3 mL/min **(E)** and 12 mL/min **(F)**. **(G)** Cell proliferation, as quantified as the percentage of *Ki-67*-positive cells as a function of flow rate at 1 and 7 days. **(H)** Cell viability, the percentage of apoptotic cells, as determined by TUNEL staining and lactase dehydrogenase concentrations in the media as function of flow rate after 1 day. Due to massive cell death experienced at 40 mL/min, experiments at this flow rate did not proceed to day 7. Results presented as mean ± SD, $n = 3$. $*p < 0.05$, $**p < 0.01$. Color images available online at www.liebertpub.com/tec

clusters and the nearest vascular channel, is linearly correlated with system pressure (Fig. 2B).

Cell occupancy 1 day after cell seeding, quantified through image analysis as the percent area of the scaffold's section surface occupied with cells, is positively correlated with flow rate (Fig. 2C). Cell occupancy 7 days postseeding peaked at 9 mL/min and decreased at 12 mL/min (Fig. 2D–F). These results suggest that the mechanical forces exerted by the system's flow act in two phases: (1) during cell seeding (measurements taken at day 1), flow primarily affects cell deposition inside the scaffold, with higher flow rates and system pressures driving cells more effectively from the vascular channels into the parenchymal spaces and (2) during the subsequent 6 days (measurements made at day 7), lower, but ''physiological,'' flow rates support the maintenance of the cells, as indicated by cell occupancy (Fig. 2D and Supplementary Fig. S1), as well as proliferation, apoptosis, and cytotoxicity (Fig. 2G, H).

Specifically, we did not observe significant differences in cell proliferation, apoptosis, and cytotoxicity 1 day postseeding between flow rates ranging from 3 to 12 mL/min (Fig. 2G, H). However, at a flow rate of 40 mL/min, there was significantly lower cell proliferation and higher apoptosis and cytotoxicity (Fig. 2G, H). The findings at 40 mL/min may be due to elevated shear stress effects, which suppressed cell proliferation and significantly increased apoptosis and cytotoxicity, demonstrating the influence of high fluid flow rates on cell survival. Accordingly, we did not include the 40 mL/min flow rate in the subsequent studies on liver tissue organization. At flow rates between 3 and 12 mL/min, cell proliferation increased between 1 and 7 days postseeding, with peaks at 6 and 9 mL/min (Fig. 2G). There were no significant changes in cell apoptosis and toxicity between 1 and 7 days postseeding for these flow rates (Fig. 2H). Collectively, these results demonstrate that the perfusion system model can deliver discrete flow rates and pressures into the liver ECM scaffold that specifically affect cellular distribution and viability inside the scaffold, in a correlative manner.

Fluid flow-derived mechanical forces control cellular organization

We next analyzed the effects of increasing fluid flow rates on cellular organization inside the ECM scaffolds. Analysis of the bioengineered liver tissue 1 day postseeding revealed a mixed population of HepG2 and MS1 in both the scaffold parenchyma and vascular channels, at all flow rates tested (Fig. 3A, top). In contrast, after 7 days of perfusion, EC were mostly localized at the vascular channels of the liver ECM scaffold, while HepG2 cells formed large cell clusters in the parenchyma (Fig. 3A, bottom). Specific staining for each cell type and cell proliferation marker, *Ki-67*, confirmed that both hepatocytic cells and EC were proliferating after 7 days (Fig. 3B).

Subsequently, we quantified cellular distribution within the vascular structures and the parenchyma using image analysis. At all flow rates tested, there were significantly more vascular structures lined with only EC at day 7 compared to day 1, suggesting that the EC migrated to the vascular channels and proliferated between days 1 and 7 (Fig. 3C). Accordingly, the number of vascular structures lined by a mixture of hepatic cells and EC significantly decreased between days 1 and 7. Similarly, there was a significant increase in the size of hepatocytic cell clusters from days 1 to 7 (Fig. 3D).

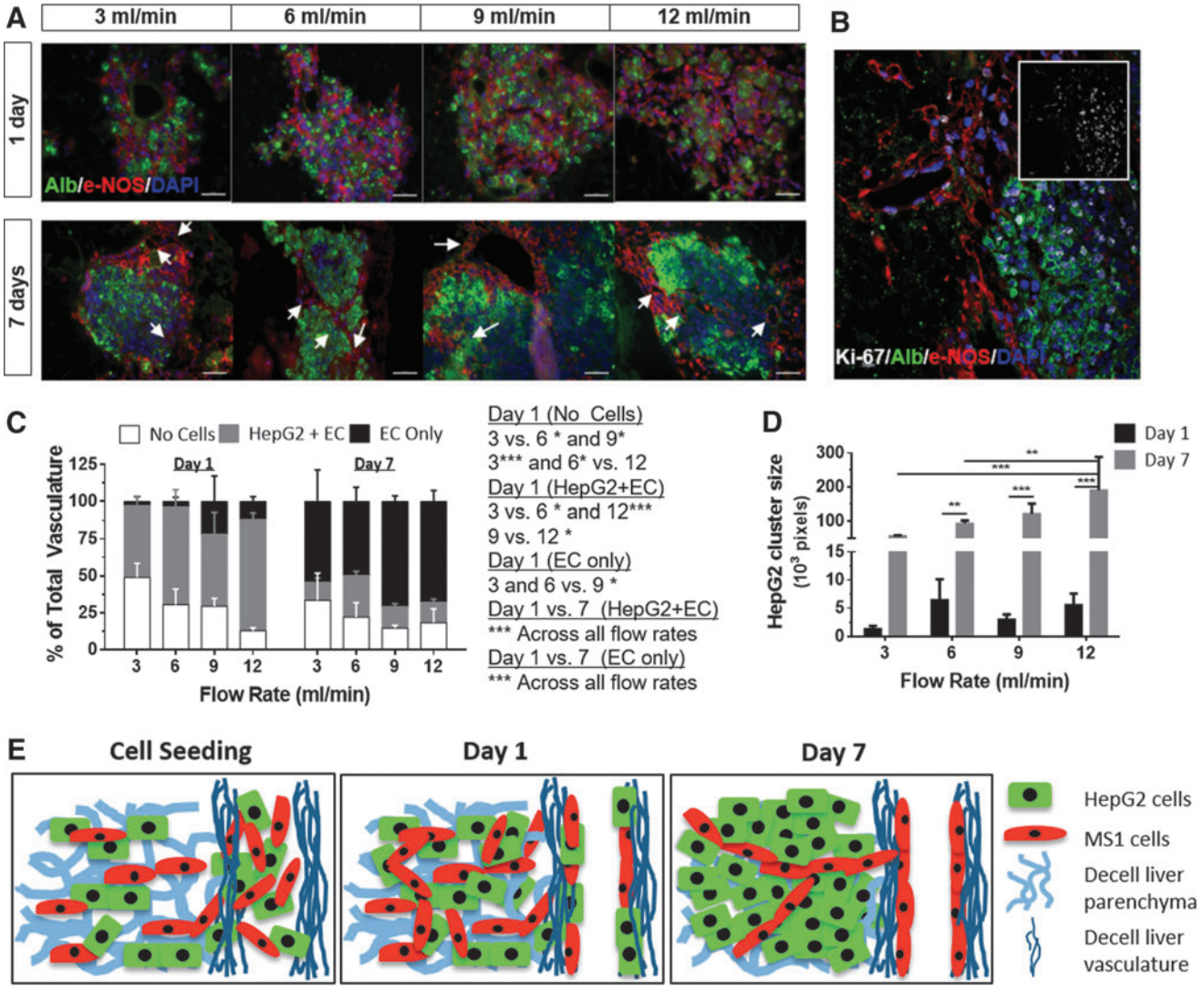

FIG. 3. Effects of fluid flow rate on cellular organization. **(A)** Representative images of albumin staining of HepG2 cells (*green*) and *eNOS* staining of MS1 cells (*red*) from days 1 (*top*) and 7 (*bottom*), at the indicated flow rates (*white arrows* point to vascular structures). **(B)** Coimmunostaining of cells expressing albumin, *eNOS* and *Ki-67* (*inset*). **(C)** Analysis of cell types (MS1+HepG2, MS1 only, and no cells) covering the vascular structures at 3, 6, 9, and 12 mL/min, 1 and 7 days postcell seeding. **(D)** HepG2 cluster size at 1 and 7 days postcell seeding. **(E)** An animation of cellular organization in the liver scaffold during perfusion seeding. Results presented as mean ± SD, $n = 3$. $*p < 0.05$, $**p < 0.01$, $***p < 0.001$. Scale bars: 100 μm **(A)**, 50 μm **(B)**. *eNOS*, endothelial nitric oxide synthase.

When comparing different flow rates, we found a significant correlation with the localization of cells in the vascular channels and the parenchyma (Fig. 3C, D). We observed an increase in vascular channel coverage at higher flow rates at day 1. In addition, there was a linear correlation between flow rate and the size of hepatocytic cell clusters, at day 7. Collectively, these results clearly show that the perfusion flow rate has a significant effect on the organization of vascular and hepatocytic structures inside the liver ECM scaffolds. Moreover, a progressive cellular niche selection, leading to liver tissue reorganization, was observed in response to specific flow rate values (Fig. 3E). The gradual lining of vascular structures by almost exclusively EC by day 7 and the presence of HepG2 cell clusters only in the parenchymal areas demonstrated the flow-mediated niche selection.

The role of the NO pathway in cellular organization

The effects of shear stress on EC are largely mediated by the NO pathway during liver regeneration postinjury.[23,24] Since the perfusion system creates a dynamic mechanical environment within the liver scaffold, it enabled us to determine if the effects of fluid flow and shear stress on cellular organization in the bioengineered livers involved this particular pathway. We first analyzed the expression of genes involved in EC response to flow-induced shear stress in media supplemented with an NO inhibitor (1 mM L-NAME) 1 day postseeding. In this experiment, it was also vital to inhibit the PG synthesis pathway with a PG inhibitor (50 μM indomethacin) to prevent a reported compensatory effect on angiogenesis and EC migration of one pathway over the other when one is pharmacologically inhibited.[24]

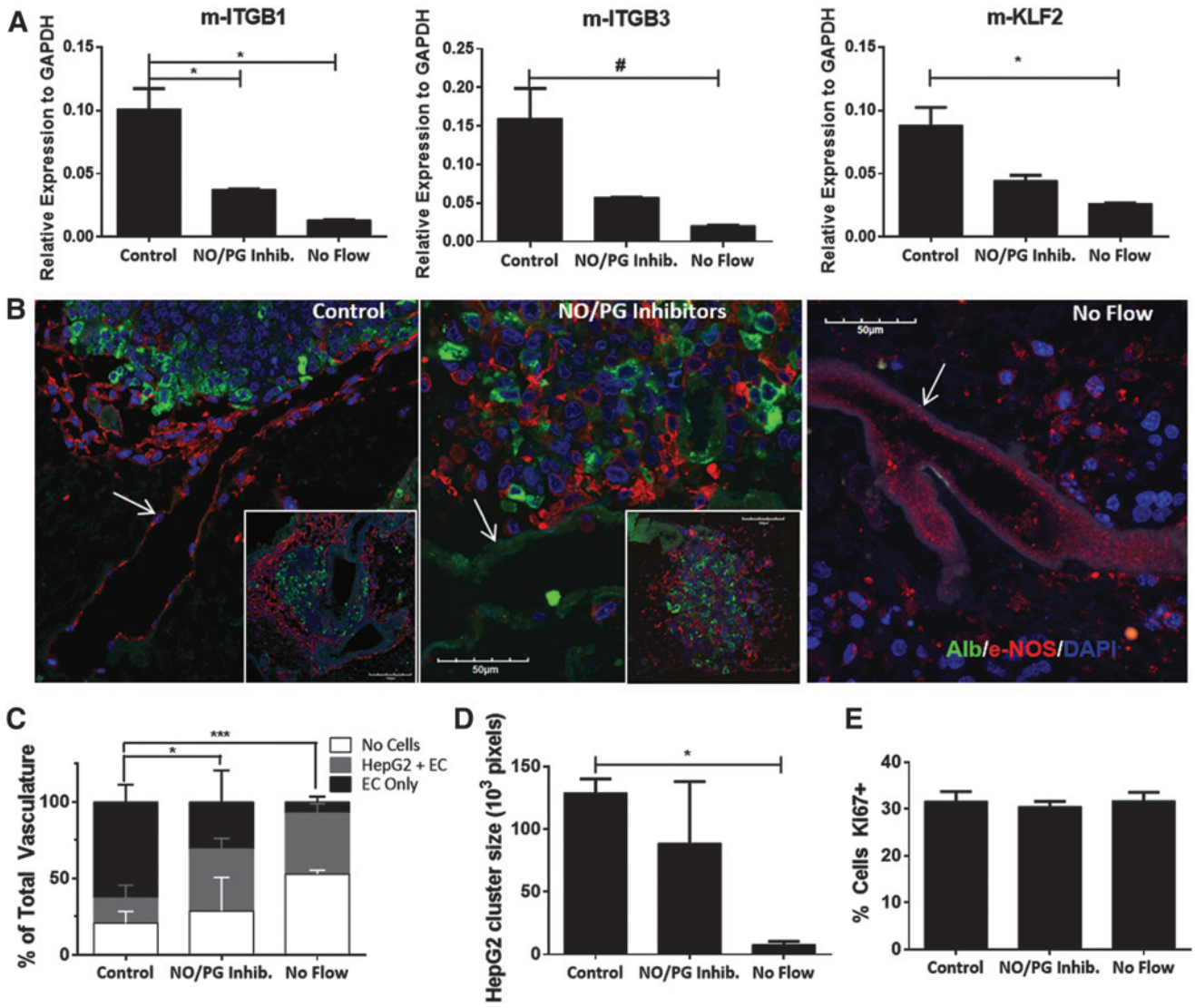

FIG. 4. NO inhibition reduces vascular and hepatocytic organization. **(A)** Quantitative PCR of RNA isolated from seeded scaffolds using standard 9 mL/min perfusion conditions (control), addition of NO and PG synthesis inhibitors (NO/PG inhibitors), and no flow conditions. Mouse-specific primers were used to analyze endothelial cell expression of *integrin β1* (*m-ITGB1*), *integrin β3* (*m-ITGB3*), and *KLF2* (*m-KLF2*). **(B)** Representative images of albumin staining of HepG2 cells (*green*) and *eNOS* staining of MS1 cells (*red*) (*white arrows* point to vascular structures covered with EC). **(C)** Analysis of cell types covering the vascular structures at 7 days postcell seeding, quantified as described in Figure 3C. Insets show low magnification images to demonstrate similar results in different areas of the liver scaffold. **(D)** HepG2 cluster size at 7 days postcell seeding **(E)** Proliferation; quantified as the percentage of *Ki-67*-positive cells. Results presented as mean ± SD, $n = 3$. $^{\#}p < 0.1$, $^{*}p < 0.05$, $^{***}p < 0.001$. EC, endothelial cells; NO, nitric oxide; PCR, polymerase chain reaction; PG, prostaglandin.

Quantitative RT-PCR using primers specific to the murine MS1 EC revealed a significant decrease in *integrin β1 (m-ITGB1)*, *β3 (m-ITGB3)*, and *KLF2 (m-KLF2)* expression under NO/PG inhibition compared to controls (Fig. 4A). To confirm that this effect was due to fluid flow inside the liver scaffold, media perfusion was stopped 1 day postseeding and the bioengineered liver constructs were maintained under ''no flow'' conditions for additional 6 days. Further decrease in the expression of these genes was observed under no flow conditions (Fig. 4A). In parallel, NO/PG synthesis inhibition affected the reorganization of cells inside the bioengineered livers and revealed a mixture of EC and HepG2 cells, with a visible reduction in organized vascular and hepatic cellular structures (Fig. 4B). Similar results of unorganized tissue structures, containing very few EC and HepG2 cells, were observed under no flow conditions (Fig. 4B).

Quantification of the histological data showed a significant decrease in the proportion of EC-coated vascular structures under NO/PG synthesis inhibition (31%), compared to controls (63%) (Fig. 4C). Under no flow conditions there were very few vascular structures lined by EC (7.1%), a significant decrease compared to control and NO/PG inhibition (Fig. 4C). In addition, there was a significant decrease in the size of HepG2 clusters in the no flow condition (7.8×10^3 pixels), compared to the control (129×10^3 pixels) (Fig. 4D). On the other hand, there was no change in cell proliferation under NO/PG synthesis inhibition and no flow conditions, suggesting that the

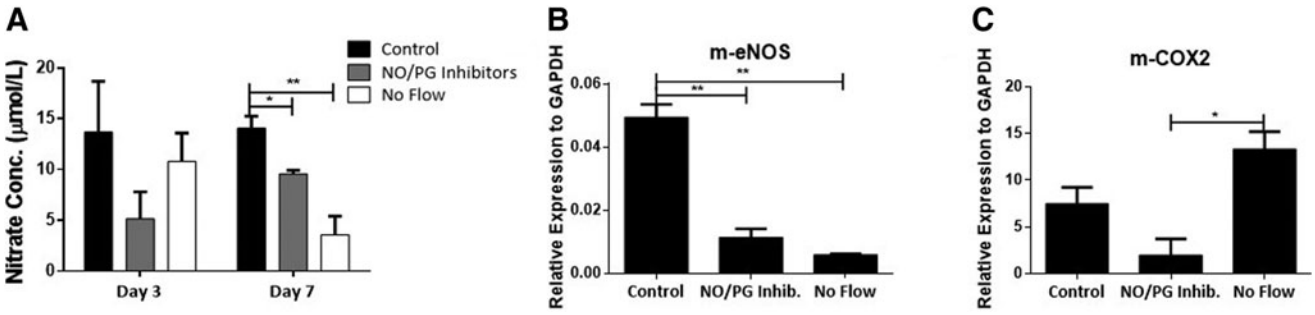

FIG. 5. Shear stress regulates EC phenotype. **(A)** Nitrate (NO) concentration in the conditioned media of liver ECM scaffolds at 3 and 7 days postcell seeding in standard perfusion conditions (control), with the addition of NO and PG synthesis inhibitors (NO/PG inhibitors), and under no flow conditions. **(B)** Quantitative PCR of mouse-specific *eNOS* (*m-eNOS*) expression under the three conditions described in **A** (7 days). **(C)** Quantitative PCR of mouse-specific *COX2* (*m-COX2*) expression under the three conditions described in **A** (7 days). Results presented as mean ± SD, $n = 3$. $^*p < 0.05$, $^{**}p < 0.01$.

decreased cellular organization is not a result of reduced cell growth under these conditions (Fig. 4E).

Measurements of NO concentrations in the bioreactor media 3 and 7 days postseeding revealed a significant decrease under NO/PG synthesis inhibition compared to controls at day 7 (Fig. 5A). There was only a modest decrease in NO concentrations under no flow conditions 3 days postseeding, which was further decreased by day 7 postseeding, suggesting a progressive adjustment of the cells to the static conditions (Fig. 5A). In addition, a significant decrease in *eNOS* expression was observed under NO synthesis inhibition and no flow conditions compared to controls (Fig. 5B). Similarly, there was also a significant decrease of *COX2* expression in EC with NO/PG inhibitors (Fig. 5C). Interestingly, in the no flow condition, there was an upregulation of this enzyme, possibly due to hypoxia in these experimental conditions.[25–27]

To confirm that the EC were the main target for the NO/PG synthesis inhibition, we incubated each cell type separately in culture dishes with the inhibitors or together in transwell dishes that allow exchange of paracrine factors without direct cell–cell interactions (Supplementary Fig. S2). There were no significant changes in NO levels for either EC or HepG2 cells, or their combination in transwell plates, with the addition of the inhibitors. Bradykinin, an inducer of NO secretion, induced a significant increase in NO synthesis, only in dishes with EC and NO/PG synthesis inhibition significantly reduced NO concentration down to its baseline, uninduced levels. As expected, HepG2 cells showed only marginal NO secretion, which was not affected by bradykinin and/or NO/PG synthesis inhibition.

These results validate the role of the NO pathway in the effects fluid flow-induced shear stress and underscore the novelty of the current model to simulate these effects *in vitro* in bioengineered liver tissues.

Discussion

Human embryonic and induced pluripotent stem cell systems can model specific hepatic tissue development[28,29]; however, they often lack the macro-organ elements such as the ECM skeleton, a native vascular tree, and organ compartmentalization. In this study, we have developed a right liver lobe perfusion system that better mimics cellular organization within a bioengineered liver construct. In particular, this system can evaluate the impact of defined mechanical forces on this process. We validated this system by demonstrating the effects of specific fluid flow rates and pressures on liver tissue growth and cellular organization. Furthermore, we validated the model by confirming the role of NO pathway in the effects of fluid flow-induced shear stress on cellular organization.

Since the acellular liver ECM scaffold preserves both the large and small vascular channels of the native organ, it is a unique system for modeling the effects of fluid flow on tissue organization.[8] For example, this system can be applied to embryonic development, where different regions are exposed to differential shear stresses and pressures.[30] As a ''proof of principle'' we tested different flow rates and found that near-physiological flow rates of 9–12 mL/min resulted in increased cell proliferation and tissue organization, while nonphysiologic hyperperfusion conditions of 40 mL/min led to cell death and 3–6 mL/min led to suboptimal tissue organization.

The choice of cells was also carefully weighted. The large amount of cells needed to perform dozens of bioreactors with different experimental flow conditions, clearly suggested that a robust cell line, easy to expand, and representative of the required cell type (and preferably vastly used in the literature) is the best choice. Rather than relying on primary cells or human embryonic/induced pluripotent stem cell-derived hepatocytes cell and EC at this point, which are still quite difficult and very expensive to generate in large numbers, we preferred more readily available cell lines, which in our opinion makes this liver modeling platform truly accessible to a larger number of scientists. Hence, HepG2, and MS1 cells fit those requirements and were the cells of choice for this initial ''proof of concept,'' since they have been extensively used as surrogates of liver cells. However, both cell types have a greater proliferation capacity than primary cells and definitive studies should employ primary liver cells.

During tissue development and regeneration, EC proliferate and migrate to form new capillaries and blood vessels.[31,32] The acellular liver ECM scaffold, inside a perfusion bioreactor, serves as a good model to study the role of fluid flow-induced shear stress on EC proliferation, migration, and organization within the vascular channels *ex vivo.* The EC migrated over a 7-day period to line the inside of the empty vascular channels inside the liver ECM scaffold[8] and were also dividing during this period. Other *ex vivo* systems that have attempted to model vascular organization are mostly

performed by coculture of EC with other cells types in 2D or 3D systems, which may include a fibrous scaffolding system, and are perfused with culture media only from the surface.[31,32] Our model has a unique advantage over these other systems in that it allows for physiological perfusion through vascular channels within the liver scaffold.

Finally, we were also able to validate a potential mechanism that mediates the effects of fluid flow on the organization of EC inside of the liver scaffold vasculature. Pharmacological suppression of NO production significantly impaired cellular organization within the scaffold, confirming the response to different flow rates or mechanical stimuli during liver development and regeneration, as previously described.[5,23,24,33–36] In addition, NO is capable of sensitizing rat adult hepatocytes for proliferation by switching them into a growth factor-responsive state through the downregulation of S-adenosylmethionine levels,[37] while on the other hand, increased oxygen and nutrient transport alone is able to increase HepG2 function and growth (i.e., cluster size).[38,39]

In our study, similar to the observations of others,[39] lowered oxygen and nutrient transport under static or low flow limited HepG2 growth. It is also possible that the lack of mechanical stimulation of the EC or *eNOS* inhibition contributed to the small size of HepG2 clusters.[1,3] Our study design was not optimal to distinguish between the effects of lack of oxygen and nutrients and the absence of mechanical stimulation under the ''No Flow'' conditions, and definitive tests can be done by analyzing the mitochondrial activity in the cells. In addition, there was also a significant decrease in the expression of EC genes that have an important role in mechanotransduction, angiogenesis, and vasculogenesis, such as *KLF2*, *eNOS*, *COX2*, *ITGB1*, and *ITGB3*, similar to the results reported by others.[40] There is the possibility that some of these effects may be due to cell stress due to lack of oxygen and nutrients in the central region of the tissue under static conditions. However, cell viability and proliferation on the outer region of the tissue were not affected by static conditions (Fig 4E), suggesting that the cells in these areas had sufficient oxygen and nutrient transport to allow cellular organization (Fig 4C, D). Also, the potential upregulation of *COX2* and *eNOS* expression under low oxygen tensions may be unrelated to mechanical stimulation.[41] Nevertheless, *eNOS* expression did not seem to be affected by hypoxia in our model (no flow condition), indicating that *eNOS* may serve as a better mechanotransducer than *COX2* in our system.

Ultimately, these findings suggest that in our bioengineered liver model, cellular organization is regulated, in part, by the *eNOS*, and COX-associated pathways. Although such finding is not necessarily new, they validate the presence of molecular mechanisms that translate mechanical stimulation cell behavior, such as cell migration and clustering. In our study, we demonstrated tissue organization impairment when the relevant molecular pathways are inhibited (the eNOS, and COX-associated pathways) and thus indicating the role of these pathways in cell migration and tissue organization inside an acellular liver scaffold (Figs. 3 and 4).

In conclusion, we described here a unique model employing an acellular intact right lobe liver ECM scaffold inside a perfusion bioreactor to test the effects of fluid flow mechanical stimulation on cellular organization inside a bioengineered liver. Unlike previously published *in vitro* models, our approach creates a simplified surrogate of a whole organ system (only two cell populations present, but with the flexibility to add more), including a branched vascular network capable of delivering a range of flow rates that provide a unique model and can be applied toward studies of human liver development and regeneration. This methodology confirmed the vital role of mechanical stimulation, mediated, in part, by NO secretion, in regulating EC organization inside the bioengineered liver. This system can be further extended to test the effects of other mechanical forces and could significantly improve the techniques for bioengineering of vascularized organs for transplantation in human patients.

Acknowledgments

This study partially supported by research grants 1R01CA180149 from the National Cancer Institute (SS), H2020-MSCA-IF-2014-660554 (PMB) and SETH/Astellas 2013 (PMB).

Disclosure Statement

No competing financial interests exist.

References

1. Matsumoto, K., Yoshitomi, H., Rossant, J., and Zaret, K.S. Liver organogenesis promoted by endothelial cells prior to vascular function. Science **294,** 559, 2001.
2. Lammert, E., Cleaver, O., and Melton, D. Induction of pancreatic differentiation by signals from blood vessels. Science **294,** 564, 2001.
3. Lammert, E., Cleaver, O., and Melton, D. Role of endothelial cells in early pancreas and liver development. Mech Dev **120,** 59, 2003.
4. Abshagen, K., Eipel, C., and Vollmar, B. A critical appraisal of the hemodynamic signal driving liver regeneration. Langenbecks Arch Surg **397,** 579, 2012.
5. Sato, Y., Koyama, S., Tsukada, K., and Hatakeyama, K. Acute portal hypertension reflecting shear stress as a trigger of liver regeneration following partial hepatectomy. Surg Today **27,** 518, 1997.
6. Sato, Y., Tsukada, K., and Hatakeyama, K. Role of shear stress and immune responses in liver regeneration after a partial hepatectomy. Surg Today **29,** 1, 1999.
7. Huh, D., Torisawa, Y.-S., Hamilton, G.A., Kim, H.J., and Ingber, D.E. Microengineered physiological biomimicry: organs-on-chips. Lab Chip **12,** 2156, 2012.
8. Baptista, P.M., Siddiqui, M.M., Lozier, G., Rodriguez, S.R., Atala, A., and Soker, S. The use of whole organ decellularization for the generation of a vascularized liver organoid. Hepatology **53,** 604, 2011.
9. Soto-Gutierrez, A., Zhang, L., Medberry, C., Fukumitsu, K., Faulk, D., Jiang, H., Reing, J., *et al.* A whole-organ regenerative medicine approach for liver replacement. Tissue Eng Part C Methods **17,** 677, 2011.
10. Bao, J., Shi, Y., Sun, H., Yin, X., Yang, R., Li, L., Chen, X., *et al.* Construction of a portal implantable functional tissue-engineered liver using perfusion-decellularized matrix and hepatocytes in rats. Cell Transplant **20,** 753, 2011.
11. Uygun, B., Soto-Gutierrez, A., Yagi, H., Izamis, M., Guzzardi, M., Shulman, C., Milwid, J., *et al.* Organ reengineering through development of a transplantable recellularized liver graft using decellularized liver matrix. Nat Med **16,** 814, 2010.
12. Barakat, O., Abbasi, S., Rodriguez, G., Rios, J., Wood, R.P., Ozaki, C., Holley, L.S., *et al.* Use of decellularized

porcine liver for engineering humanized liver organ. J Surg Res **173,** E11, 2012.
13. Yagi, H., Fukumitsu, K., Fukuda, K., Kitago, M., Shinoda, M., Obara, H., Itano, O., *et al.* Human-scale whole-organ bioengineering for liver transplantation: a regenerative medicine approach. Cell Transplantat **22,** 231, 2013.
14. Pollack, G.M., Brouwer, K.L., Demby, K.B., and Jones, J.A. Determination of hepatic blood flow in the rat using sequential infusions of indocyanine green or galactose. Drug Metab Dispos **18,** 197, 1990.
15. Davies, B., and Morris, T. Physiological parameters in laboratory animals and humans. Pharm Res **10,** 1093, 1993.
16. Moran, E.C., Baptista, P.M., Evans, D.W., Soker, S., and Sparks, J.L. Evaluation of parenchymal fluid pressure in native and decellularized liver tissue. Biomed Sci Instrum **48,** 303, 2012.
17. Fukuchi, T., Hirose, H., Onitsuka, A., Hayashi, M., Senga, S., Imai, N., Shibata, M., *et al.* Effects of portal-systemic shunt following 90% partial hepatectomy in rats. J Surg Res **89,** 126, 2000.
18. Baptista, P.M., Vyas, D., Moran, E., Wang, Z., and Soker, S. Human liver bioengineering using a whole liver decellularized bioscaffold. Methods Mol Biol **1001,** 289, 2013.
19. Yang, Y.Z., Yang, Y.S., Xu, Y., Lick, S.D., Awasthi, Y.C., and Boor, P.J. Endothelial glutathione-S-transferase A4-4 protects against oxidative stress and modulates NOS expression through NF-kappa B translocation. Toxicol Appl Pharmacol **230,** 187, 2008.
20. Wang, L., Yang, Y., Dwivedi, S., Xu, Y., Chu, E.T., Li, J., Fitchett, K., *et al.* Manipulating glutathione-S-transferases may prevent the development of tolerance to nitroglycerin. Cardiovasc Toxicol **6,** 131, 2006.
21. Huch, M., Gehart, H., van Boxtel, R., Hamer, K., Blokzijl, F., Verstegen, M.M.A., Ellis, E., *et al.* Long-term culture of genome-stable bipotent stem cells from adult human liver. Cell **160,** 299, 2015.
22. Knowles, B.B., Howe, C.C., and Aden, D.P. Human hepatocellular-carcinoma cell-lines secrete the major plasma-proteins and hepatitis-B surface-antigen. Science **209,** 497, 1980.
23. Schoen, J.M., Wang, H.H., Minuk, G.Y., and Lautt, W.W. Shear stress-induced nitric oxide release triggers the liver regeneration cascade. Nitric Oxide **5,** 453, 2001.
24. Schoen Smith, J.M., and Lautt, W.W. The role of prostaglandins in triggering the liver regeneration cascade. Nitric Oxide **13,** 111, 2005.
25. Colgan, S.P., Taylor, C.T., Narravula, S., Synnestvedt, K., and Blume, E.D. Endothelial COX-2 induction by hypoxia liberates 6-keto-PGF1 alpha, a potent epithelial secretagogue. Adv Exp Med Biol **507,** 107, 2002.
26. Inoue, H., Taba, Y., Miwa, Y., Yokota, C., Miyagi, M., and Sasaguri, T. Induction of cyclooxygenase-2 expression by fluid smear stress in vascular endothelial cells. Adv Exp Med Biol **525,** 141, 2003.
27. Wu, G., Luo, J., Rana, J.S., Laham, R., Sellke, F.W., and Li, J. Involvement of COX-2 in VEGF-induced angiogenesis via P38 and JNK pathways in vascular endothelial cells. Cardiovasc Res **69,** 512, 2006.
28. Zhu, Z., and Huangfu, D. Human pluripotent stem cells: an emerging model in developmental biology. Development **140,** 705, 2013.
29. Takebe, T., Sekine, K., Enomura, M., Koike, H., Kimura, M., Ogaeri, T., Zhang, R.-R., *et al.* Vascularized and functional human liver from an iPSC-derived organ bud transplant. Nature **499,** 481, 2013.
30. Collardeau-Frachon, S., and Scoazec, J.-Y. Vascular development and differentiation during human liver organogenesis. Anat Rec **291,** 614, 2008.
31. Ucuzian, A.A., and Greisler, H.P. *In vitro* models of angiogenesis. World J Surg **31,** 654, 2007.
32. Morin, K.T., and Tranquillo, R.T. *In vitro* models of angiogenesis and vasculogenesis in fibrin gel. Exp Cell Res **319,** 2409, 2013.
33. Cantre, D., Schuett, H., Hildebrandt, A., Dold, S., Menger, M.D., Vollmar, B., and Eipel, C. Nitric oxide reduces organ injury and enhances regeneration of reduced-size livers by increasing hepatic arterial flow. Br J Surg **95,** 785, 2008.
34. Mei, Y., and Thevananther, S. Endothelial nitric oxide synthase is a key mediator of hepatocyte proliferation in response to partial hepatectomy in mice. Hepatology **54,** 1777, 2011.
35. Diaz-Juarez, J., and Hernandez-Munoz, R. The role of calcium and nitric oxide during liver enzyme release induced by increased physical forces as evidenced in partially hepatectomized rats. Liver Transplant **17,** 334, 2011.
36. Yoshida, D., Akahoshi, T., Kawanaka, H., Yamaguchi, S., Kinjo, N., Taketomi, A., Tomikawa, M., *et al.* Roles of vascular endothelial growth factor and endothelial nitric oxide synthase during revascularization and regeneration after partial hepatectomy in a rat model. Surg Today **41,** 1622, 2011.
37. Garcia-Trevijano, E.R., Martinez-Chantar, M.L., Latasa, M.U., Mato, J.M., and Avila, M.A. NO sensitizes rat hepatocytes to proliferation by modifying S-adenosylmethionine levels. Gastroenterology **122,** 1355, 2002.
38. Tanaka, Y., Yamato, M., Okano, T., Kitamori, T., and Sato, K. Evaluation of effects of shear stress on hepatocytes by a microchip-based system. Meas Sci Technol **17,** 3167, 2006.
39. Anada, T., Fukuda, J., Sai, Y., and Suzuki, O. An oxygen-permeable spheroid culture system for the prevention of central hypoxia and necrosis of spheroids. Biomaterials **33,** 8430, 2012.
40. Ha, C.H., Kim, S., Chung, J., An, S.H., and Kwon, K. Extracorporeal shock wave stimulates expression of the angiogenic genes via mechanosensory complex in endothelial cells: mimetic effect of fluid shear stress in endothelial cells. Int J Cardiol **168,** 4168, 2013.
41. Searles, C.D. Transcriptional and posttranscriptional regulation of endothelial nitric oxide synthase expression. Am J Physiol Cell Physiol **291,** C803, 2006.

Address correspondence to:
Pedro M. Baptista, PharmD, PhD
Instituto de Investigación Sanitaria de Aragón (IIS Aragón)
Avda. San Juan Bosco, 13
Zaragoza 50009
Spain

E-mail: pbaptista.iacs@aragon.es

Shay Soker, PhD
Wake Forest Institute for Regenerative Medicine
Wake Forest University Health Sciences
Winston-Salem, NC 27157

E-mail: ssoker@wakehealth.edu

Received: July 17, 2015
Accepted: November 30, 2015
Online Publication Date: February 12, 2016